A General Method for Solvent Exchange of Plasmonic Nanoparticles and Self-Assembly into SERS-Active Monolayers

Ana B. Serrano-Montes,[†] Dorleta Jimenez de Aberasturi,*[,†] Judith Langer,[†] Juan J. Giner-Casares,[†] Leonardo Scarabelli,[†] Ada Herrero,[†] and Luis M. Liz-Marzán*[,†,‡]

[†]CIC biomaGUNE, Paseo de Miramón 182, 20009 Donostia-San Sebastián, Spain

[‡]Ikerbasque, Basque Foundation for Science, 48013 Bilbao, Spain

*e-mail: djimenezdeaberasturi@cicbiomagune.es; llizmarzan@cicbiomagune.es

SUPPLEMENTARY INFORMATION

1. Nuclear Magnetic Resonance (NMR) studies

In order to characterize the ligands present on the surface of the nanoparticles after phase transfer process an NMR study has been carried with 50nm Au NPs. *^{1}H* NMR spectra were acquired on Bruker 500MHz spectrometer. Chemical shifts were reported in ppm (δ) and splitting patterns are designated as "s", singlet; "t", triplet; "q", quadruplet; and "m", multiplet. The residual signals of the deuterated solvent correspond to Methanol-d4 4.87 ppm; Chloroform-d 7.26 ppm.

The spectra of free ligands are shown in **Figure S1A**: **I**) PEG-SH; **II**) DDT. Signal assignments are shown below.

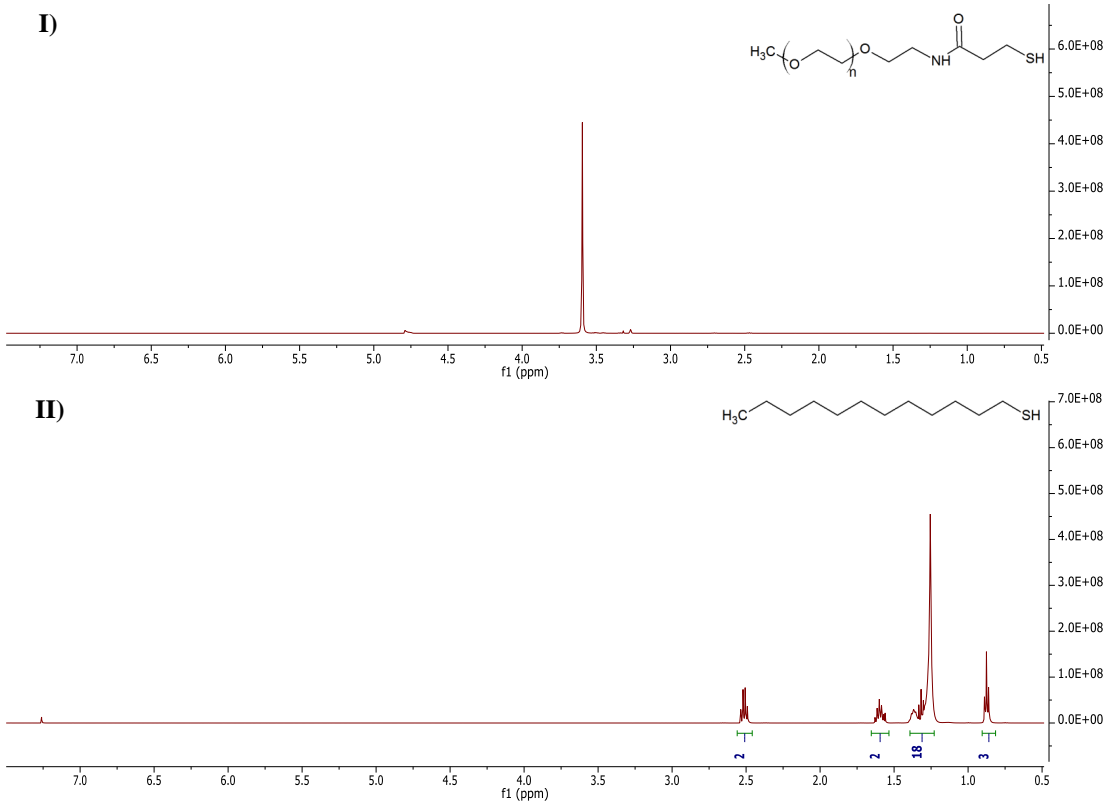

Figure S1A. ^{1}H NMR spectra of: **I**) PEG-SH ^{1}H NMR (500 MHz, Methanol-d4) δ 3.64 (s, PEG-SH). The main peak in the spectrum corresponds to polyethylene glycol protons. **II**) DDT ^{1}H NMR (500 MHz, Chloroform-d) δ 2.51 (q, 2H, C**H$_2$**SH), 1.64 – 1.55 (m, 2H, C**H$_2$**CH$_2$SH), 1.39 – 1.21 (m, 18H, 9CH$_2$), 0.88 (t, 3H, CH$_3$).

In addition, the ^{1}H NMR spectra of surface bound ligands are shown in **Figure S1B**. Spectrum **III** corresponds to a mixture of DDT and PEG-SH, in the same ratio used for the functionalization of the gold nanoparticles measured in spectrum **IV**. We found that the spectrum of 50 nm Au-NP capped with DDT and PEG-SH (**IV**) does show the peaks of both ligands on the nanoparticle surface, confirming their presence after phase transfer. Some features in the ^{1}H NMR indicate that the ligands are attached to the nanoparticle: i) Chemical shift and broadening observed in the signals; ii) Perfect fit in the assignment of the number of protons for free DDT (**2** and **3)**; iii) The absence of peaks (2.5 ppm) corresponding to protons close to the metal core indicates complete removal of free ligands.

Interestingly, integration of the two main peaks of each ligand (**1** and **2**) allowed us to estimate their ratio on the nanoparticle surface. In this case, for the initial ligand ratio corresponding to 1.3 % of PEG (spectrum **III**) we found that after NPs phase transfer and washing the integral of the PEG signal (**1**) decreases (spectrum **IV)**, remaining only 1% of PEG with respect to DDT on the NP surface. This suggests that the ligand ratio can vary slightly upon phase transfer due to the use of excess DDT, which may lead to ligand exchange in a small extent.

A complementary study was carried out by etching the functionalized nanoparticles, as previously reported.[1] Complete oxidation of AuNPs with potassium cyanide was achieved, as evidenced by a color change in solution from red to colorless. Spectrum (**V**) in **Figure S1B** shows the main signals of the ligands (**1** for PEG-SH) and (**2, 3** for DDT) after etching with cyanide. Both spectra (**IV** and **V**) confirm functionalization of 50nm AuNPs with both PEG- SH and DDT after phase transfer.

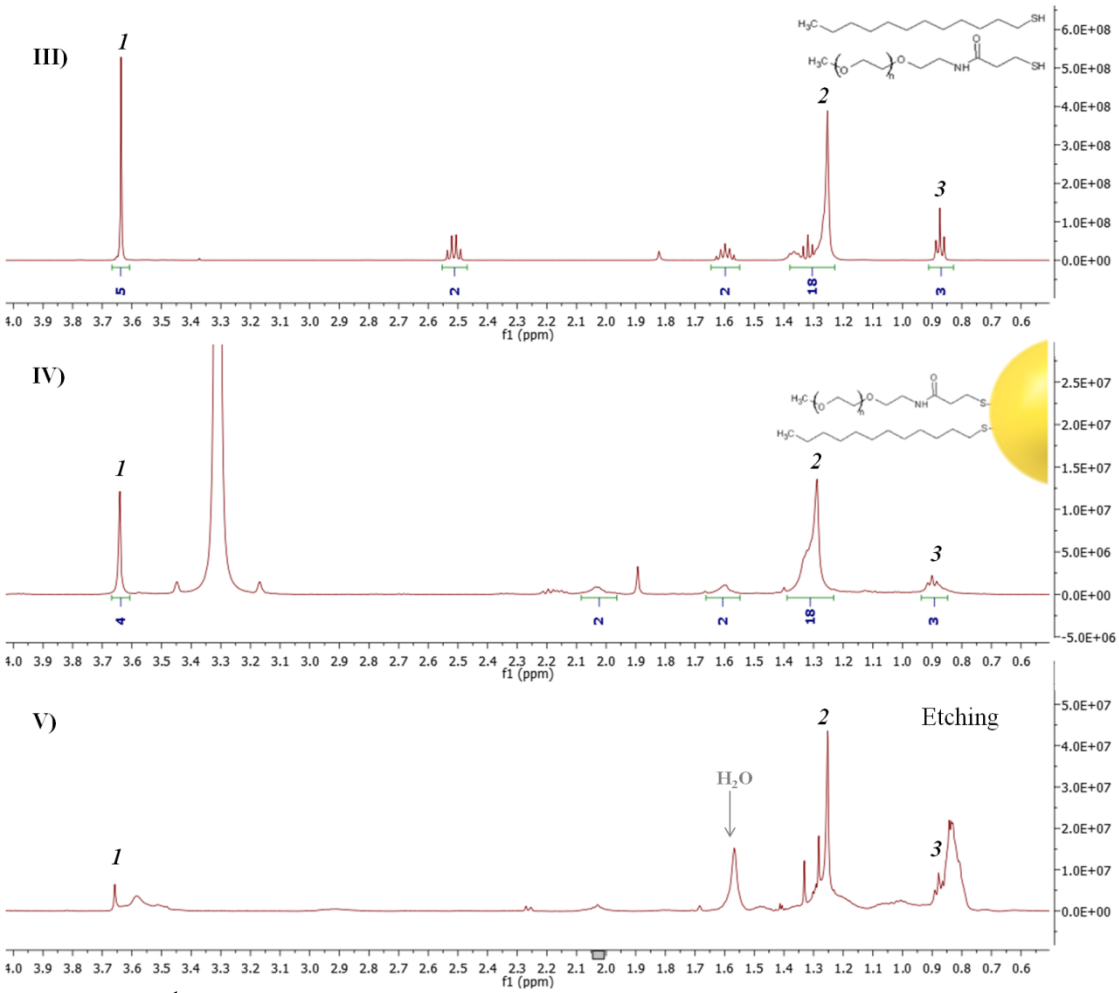

Figure S1B. ^{1}H NMR spectra of: **III**) PEG-DDT (500 MHz, Chloroform-d) δ 3.64 (s, PEG-SH), 2.51 (q, 2H, C**H$_2$**SH), 1.64 – 1.55 (m, 2H, C**H$_2$**CH$_2$SH), 1.39 – 1.21 (m, 18H, 9CH$_2$), 0.88 (t, 3H, CH$_3$). **IV**) 50nm AuNPs (PEG-DDT) in Methanol-d4, acquisition time 1h. The peaks of the ligands on the NPs correspond well with those observed in spectrum (**III**). **V**) PEG-DDT ligands in Chloroform-d after cyanide oxidation of 50nm AuNPs, acquisition time 40min.

2. Vis-NIR spectra, TEM images and size distribution histograms

2.1 Gold spheres

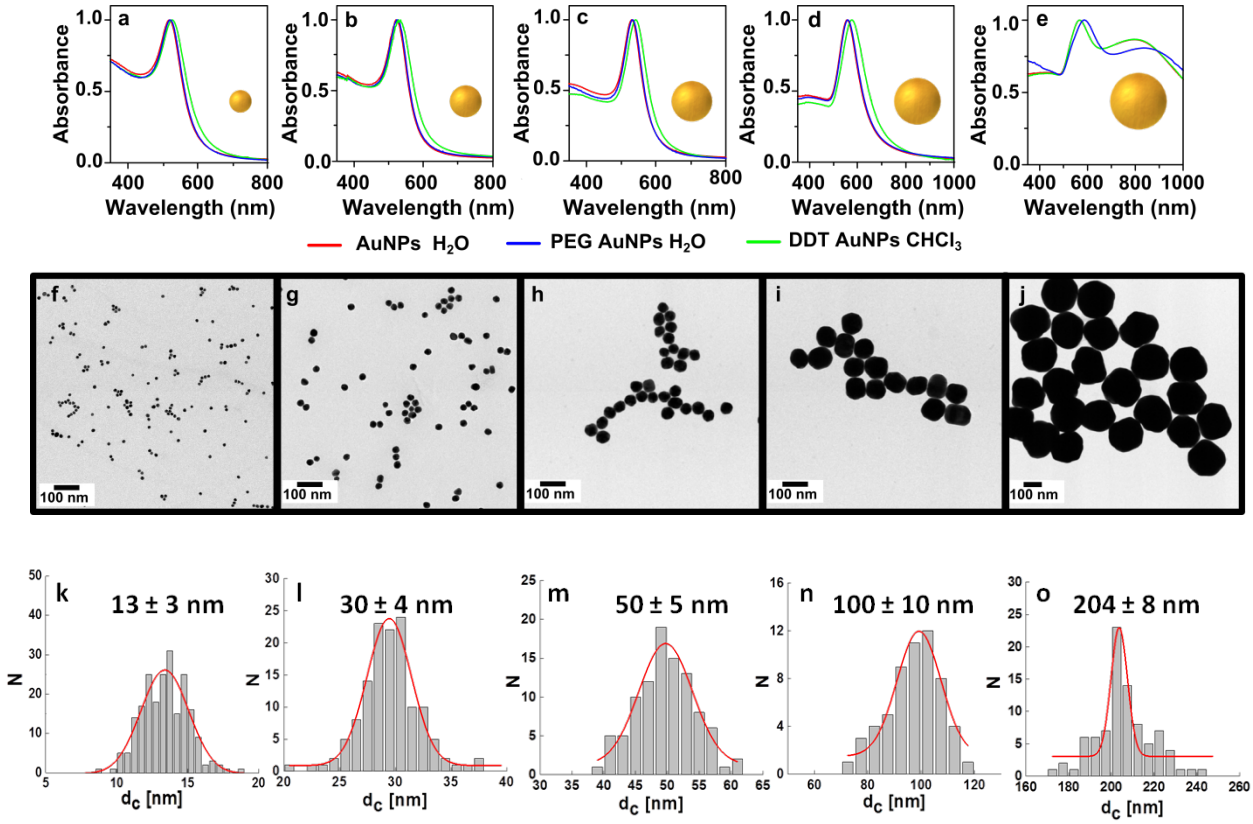

Figure S2. (**a-e**) Vis-NIR spectra of AuNPs in water (red lines), after addition of PEG-SH in water (blue lines) and after coating with PEG/DDT and transfer into $CHCl_3$ (green lines). TEM images (**f-j**) and size distribution histograms (**k-o**) of PEG/DDT coated nanoparticles: AuNP seeds (**f**, **k**), Au 30 (**g**, **l**), Au 50 (**h**, **m**), Au 100 (**i**, **n**) and Au 200 (**j**, **o**).

2.2 Silver spheres

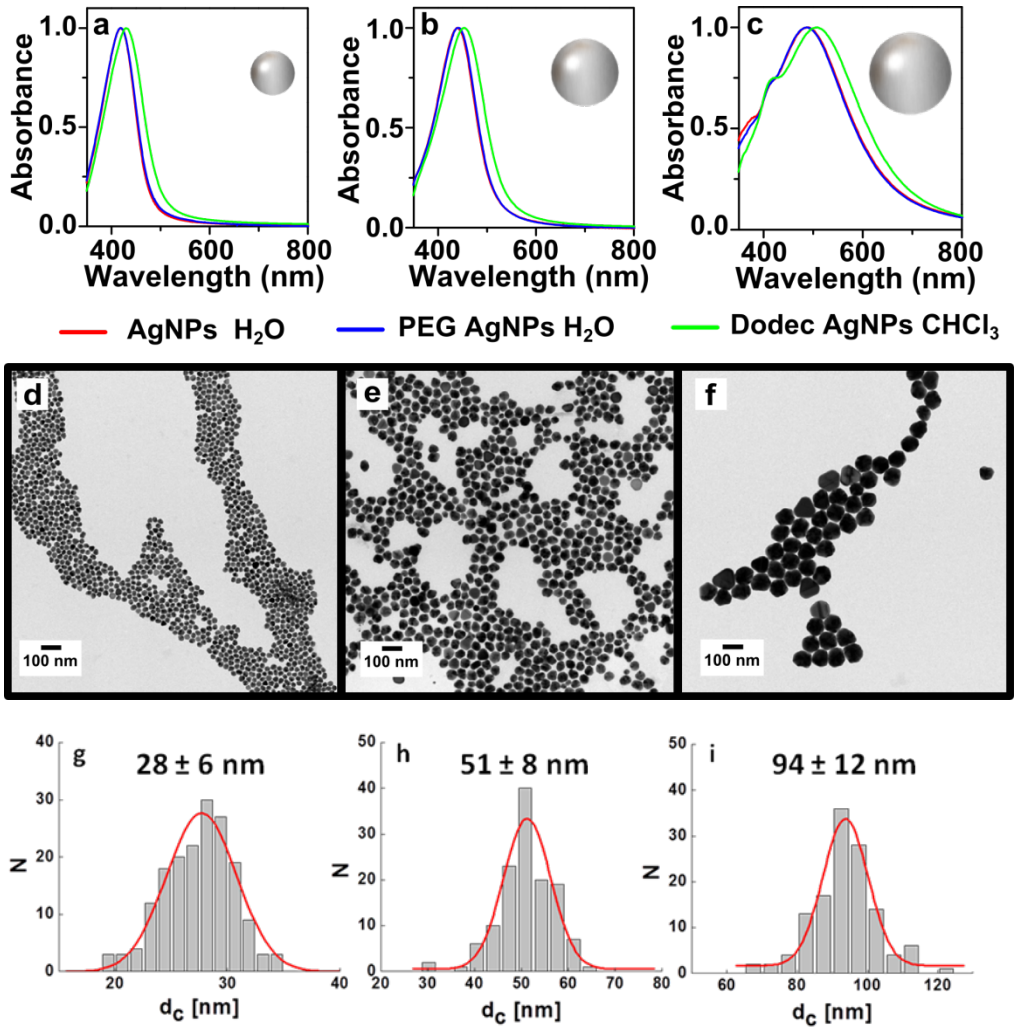

Figure S3. (a-c) UV-Vis-NIR spectra of Ag 30 (**a**), Ag 50 (**b**) and Ag 100 (**c**) in water (red lines), after addition of PEG-SH in water (blue lines) and after coating with PEG/DDT and transfer into $CHCl_3$ (green lines). TEM images (**d-f**) and size distribution histograms (**g-h**) of PEG/DDT coated nanoparticles: Ag 30 (**d**, **g**), Ag 50 (**e**, **h**) and Ag 100 (**f**, **i**).

2.3 Gold nanostars

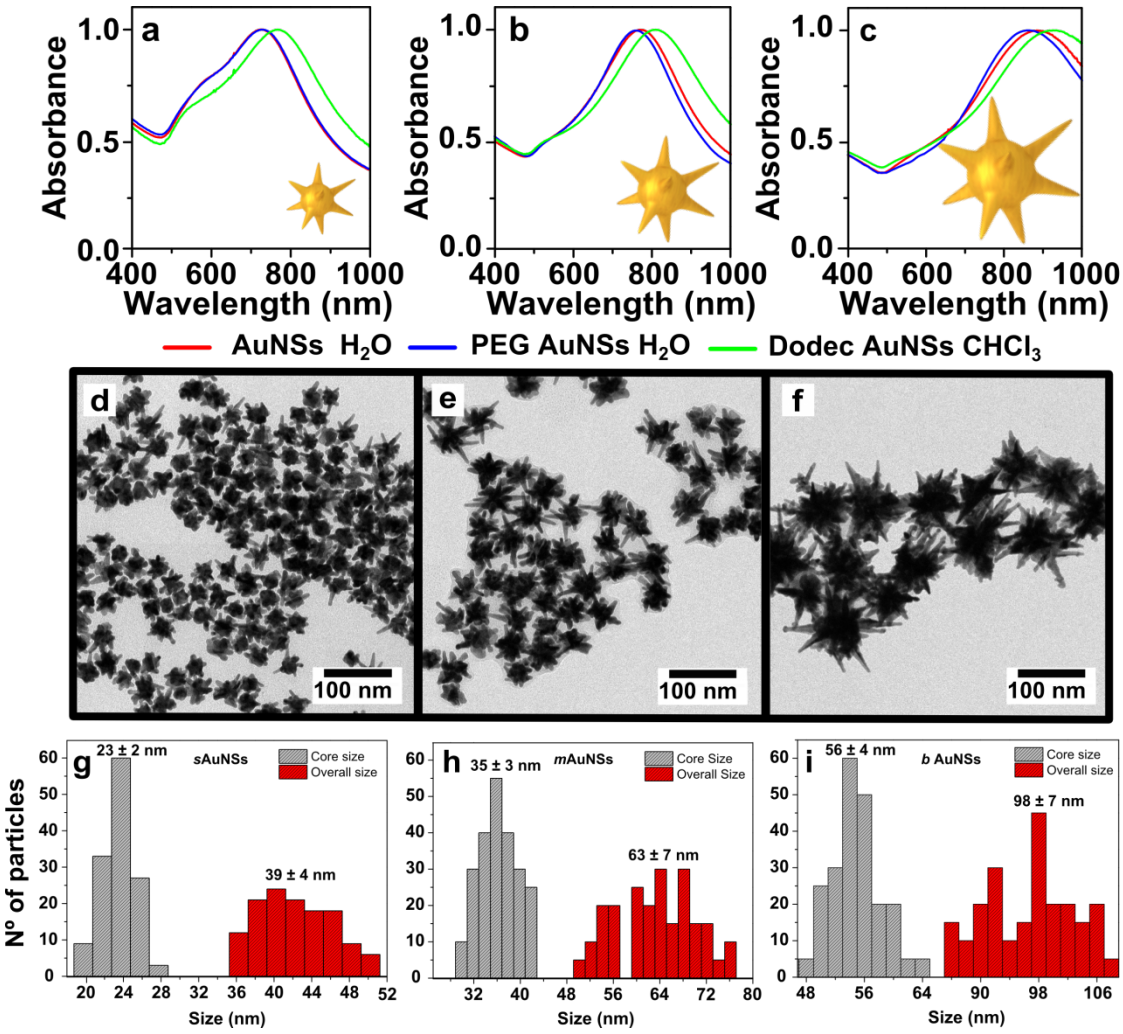

Figure S4. (a-c): UV-Vis-NIR spectra of *s*AuNSs (**a**), *m*AuNSs (**b**) and *b*AuNSs (**c**) in water (red lines), after addition of PEG-SH in water (blue lines) and after coating with PEG/DDT and transfer into $CHCl_3$ (green lines). TEM images (**d-f**) and histograms (**g-h**) showing the core (green bars) and overall size (red bars), for PEG/DDT coated nanoparticles: *s*AuNSs (**d**, **g**), *m*AuNSs (**e**, **h**) *b*AuNSs (**f**, **i**).

3. Stability of silver nanoparticles

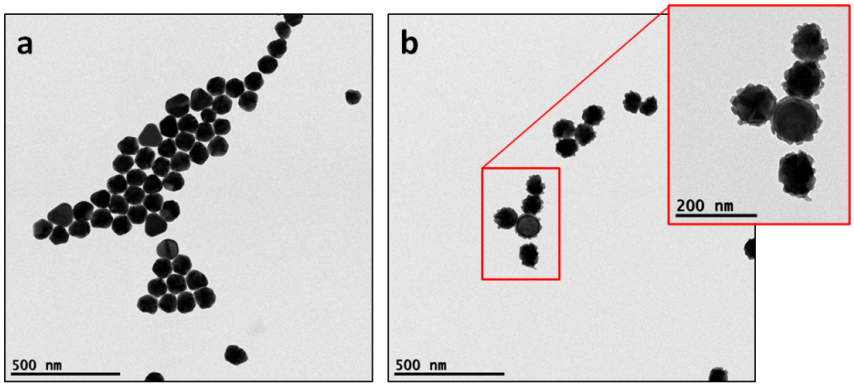

Figure S5. TEM images of Ag 100 after PEG/DDT coating (**a**) and after 2 months in contact with air on the TEM grid (**b**). The inset shows the morphological changes due to Ag oxidation after drying on solid substrates.

4. Vis-NIR spectral evolution of gold nanostars

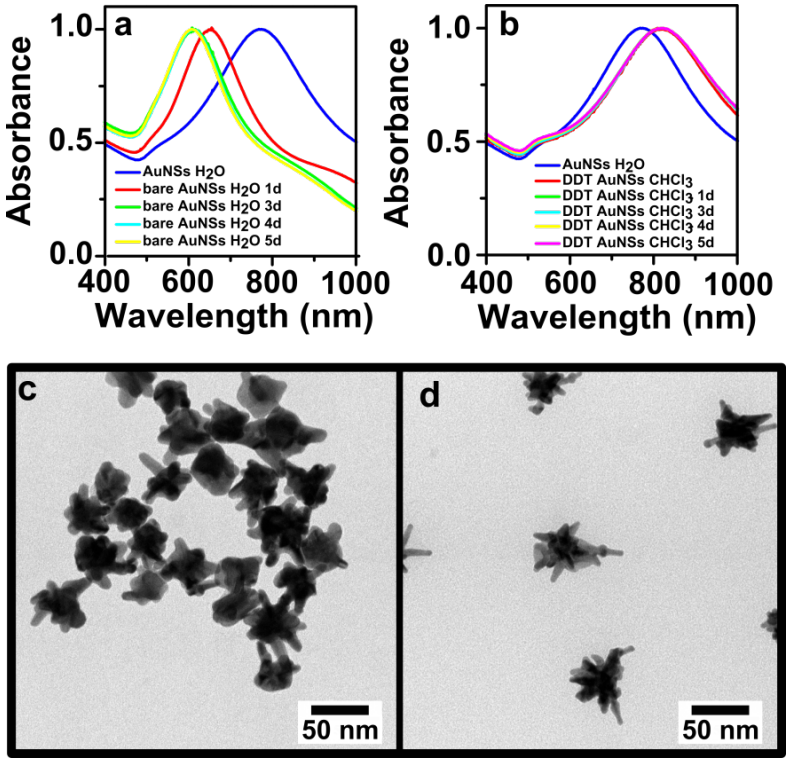

Figure S6. UV-Vis-NIR spectral evolution (**a**-**b**) and TEM images (**c**-**d**) of bare (**a**, **c**) and PEG/DDT coated *m*AuNSs (**b**, **d**), 5 days after synthesis. Without coating the LSPR band blueshifts (**a**) and nanostars become more rounded (**c**). Upon PEG/DDT capping and phase transfer into chloroform, no LSPR shift was observed (**b**) and the tips remained sharp due to surface passivation by Au-S bonds (**d**).

5. Solubility in different solvents

Figure S7. (a-d) Vis-NIR spectra of PEG/DDT-coated AuNRs and *m*AuNSs dispersed in different organic solvents. As previously reported,[2] the plasmon band shows a linear shift with solvent refractive index, which was not observed in hexane due the low solubility of PEG in this solvent (**Figure S7e**). Such a poor solubility in non-polar solvents as hexane or toluene can be improved by reducing the amount of PEG-SH and keeping constant the concentration of DDT. Thus, less broadened LSPR bands were obtained for lower PEG/DDT ratios. Due to the broadened plasmon bands of AuNSs, the effect of solvent exchange on the corresponding LSPR shift was not so evident.

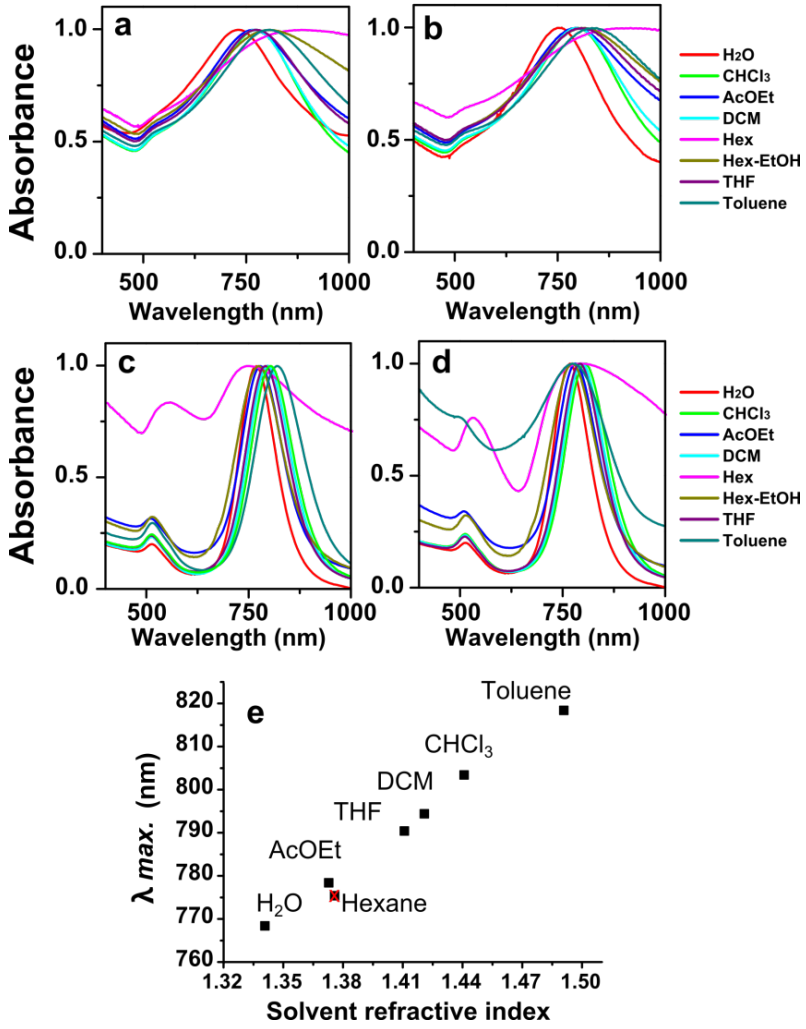

Figure S7. (**a**-**d**) Vis-NIR spectra of *m*AuNSs (**a**, **b**) and AuNRs (**c**, **d**) in different organic solvents. The NPs in (**a**, **c**) were coated with double amount of PEG-SH than those in (**b**, **d**). (**e**) Maximum LSPR wavelength as function of solvent refractive index as shown in "**d**".

6. Vis-NIR spectra of different substrates

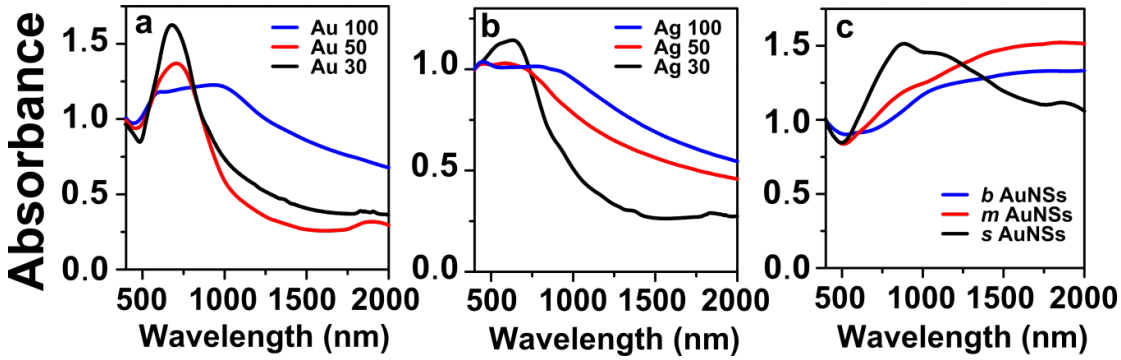

Figure S8. Vis-NIR spectra of monolayers made of AuNPs (**a**), AgNPs (**b**) and AuNSs (**c**) of different sizes.

7. Low magnification TEM and SEM images

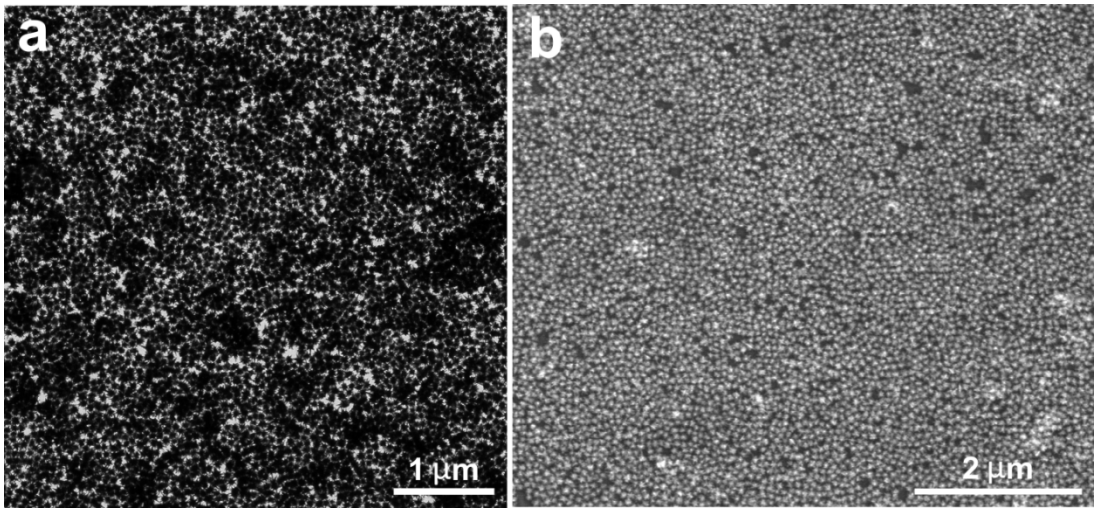

Figure S9. Large scale TEM (**a**) and SEM (**b**) images of *b*AuNS monolayers fabricated by self-assembly of PEG/DDT coated nanoparticles at the air-liquid interface.

8. SERS measurements

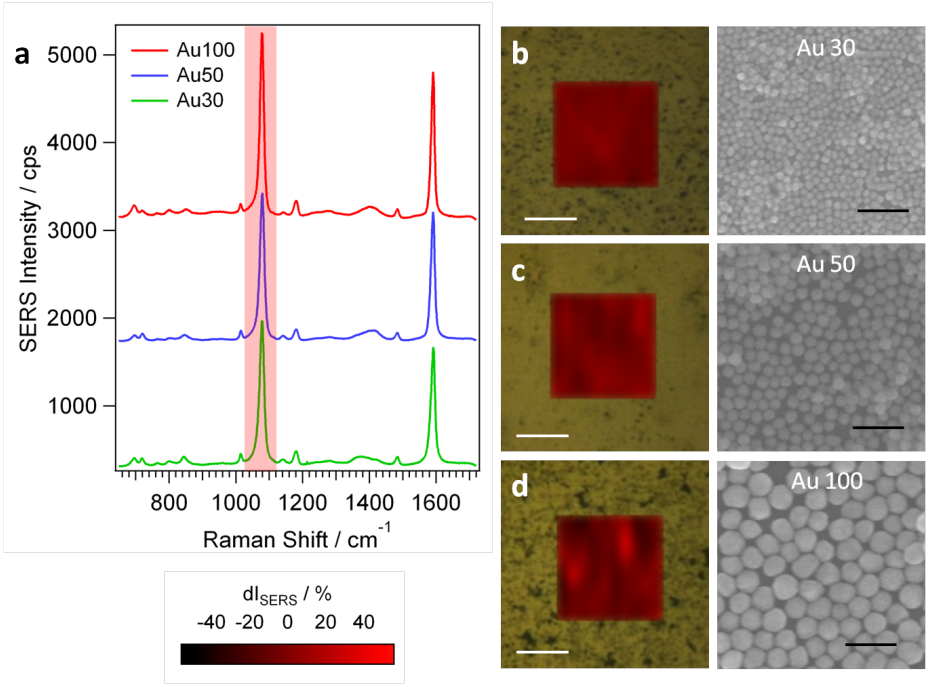

Figure S10. (**a**) Characteristic SERS spectra of 4-MBA (concentration 10 μM) on self-assembled AuNPs with different diameters, as labeled. Individual SERS spectra were measured with excitation at 785 nm, power of 200 mW and 1s collection time. SERS spectra were generated by averaging 100 single spectra from a 20x20 μm^2 grid within a point distance of 2μm in both x- and y- directions. (**b-d**) Optical and SEM images of self-assembled AuNP monolayers, as labeled. The white bars in the optical images correspond to 10μm, the black bars in SEM images are 200 nm. SERS maps show the spatial homogeneity through the 4-MBA vibration at 1078 cm^{-1} for each sample (red-shaded peaks in **a**), presented as function of the deviation dI (in %) from the average signal.

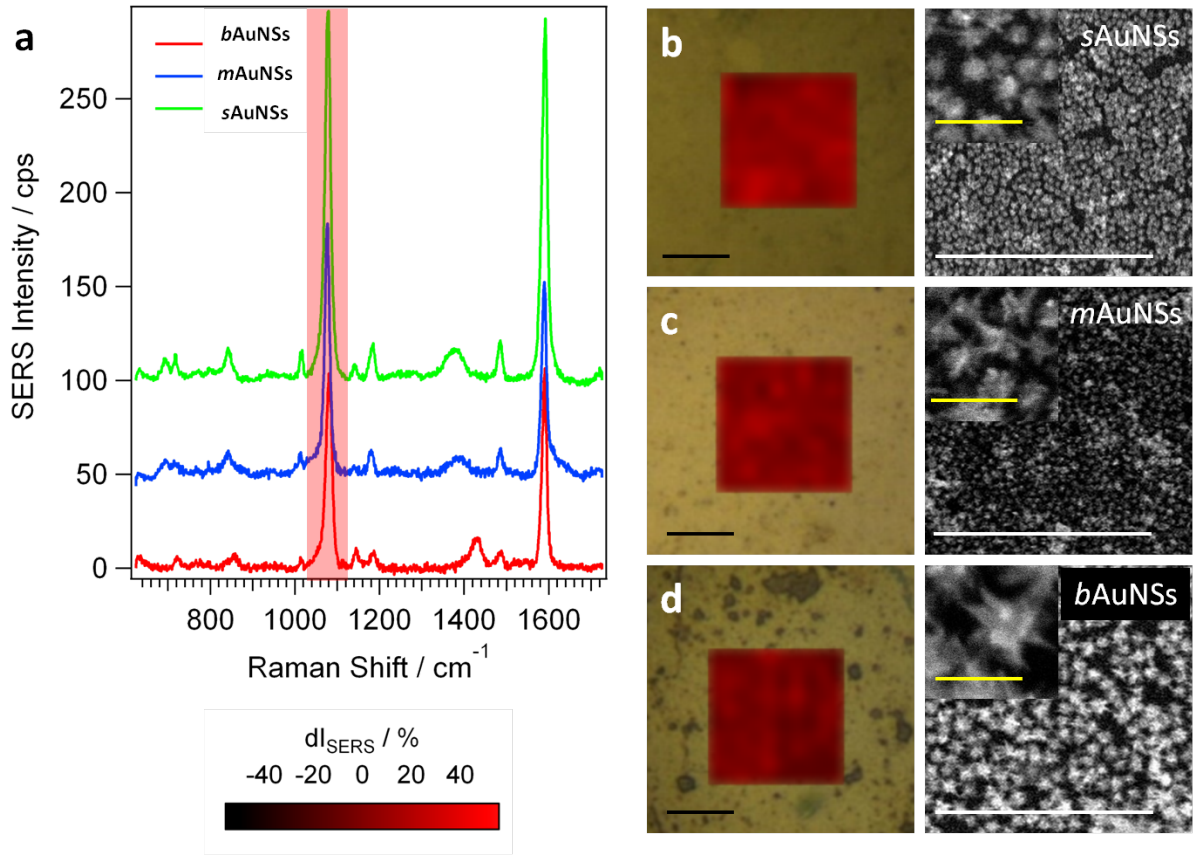

Figure S11. (**a**) Averaged SERS spectra of 4-MBA (10 μM) on assemblies of AuNSs with different diameters, as labeled. (**b-d**) Corresponding SERS maps for the signal at 1078 cm^{-1} (red-shaded peaks in (**a**)), as a function of the deviation from the average signal dI (in %) of *s*AuNSs (**b**), *m*AuNSs (**c**) and *b*AuNSs (**d**), and representative SEM images of the assemblies before incubation with the analyte.

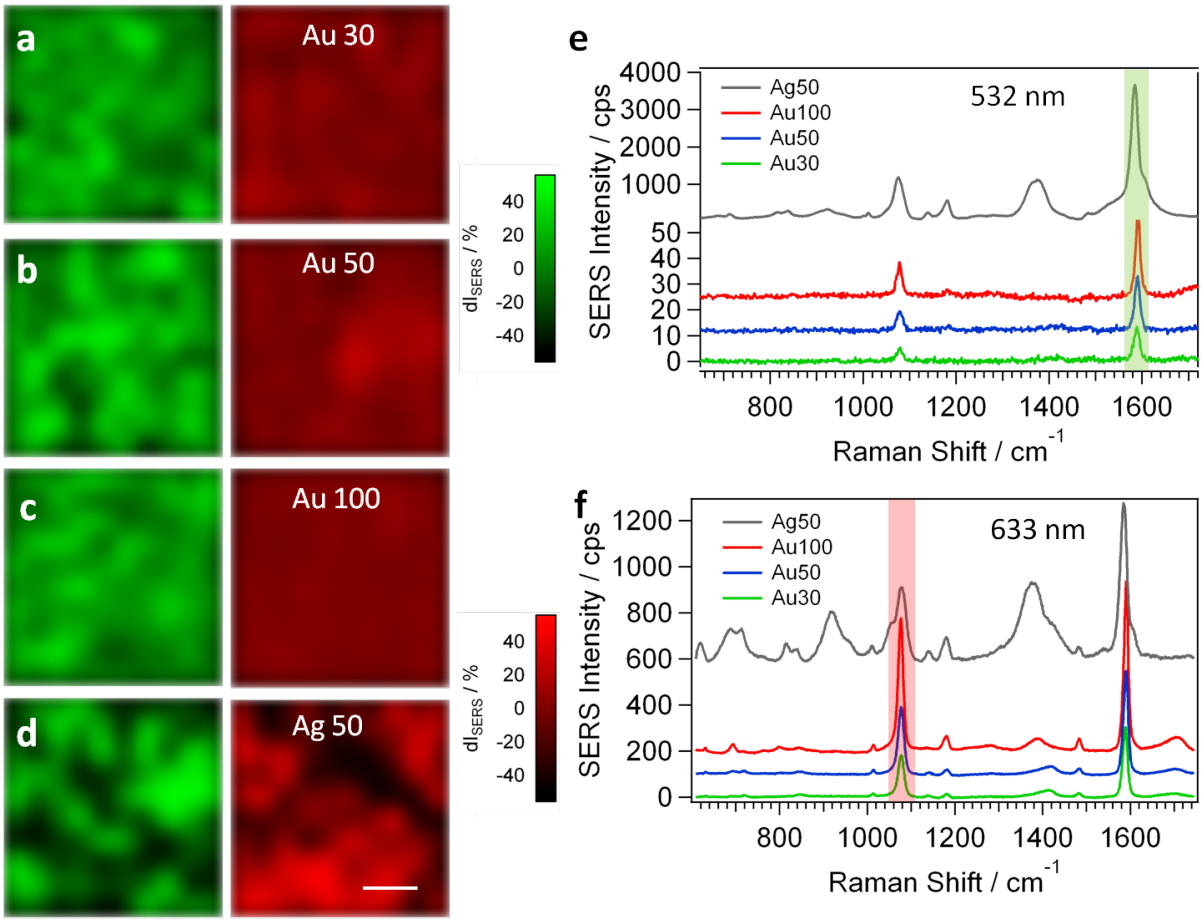

Figure S12. Averaged 4-MBA SERS spectra (10 μM) on Au 30 (**a**), Au 50 (**b**), Au 100 (**c**) and Ag 50 (**d**) monolayers, with excitation at 532 and 633 nm, and corresponding SERS maps at 1585 cm^{-1} (green scale, green-shaded peaks in **e**) for 532 nm and 1078 cm^{-1} (red scale, red-shaded peaks in **f**) for 633nm, as a function of the average intensity deviation dI (in %). Corresponding averaged SERS spectra at 532 nm and 633 nm are plotted in (**e**) and (**f**), respectively.

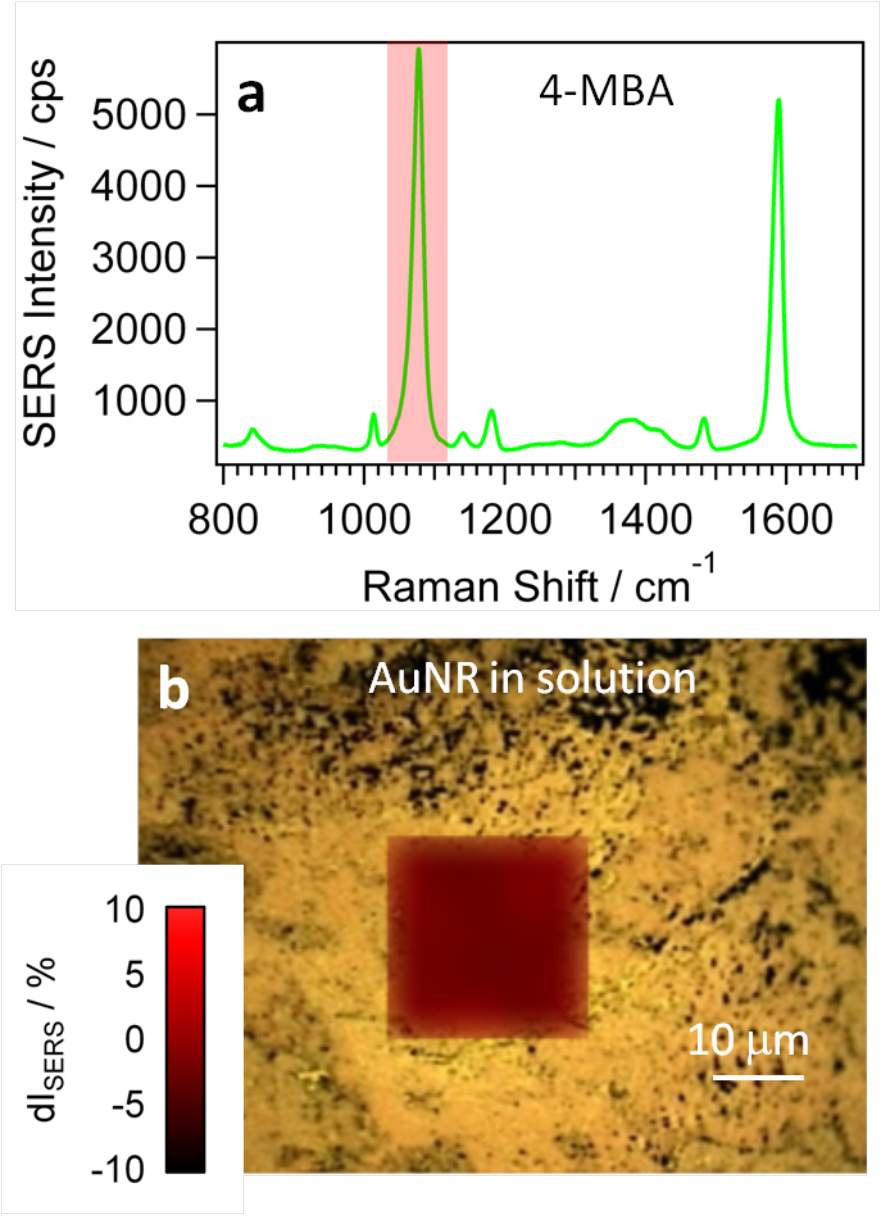

Figure S13. (**a**) Averaged SERS spectrum of 4-MBA (10 μM) on a AuNR monolayer immersed in water, excited at 785 nm;(**b**) corresponding SERS map at 1078 cm^{-1} (red scale, red-shaded peaks in **a**, as function of the average intensity deviation dI in %.

Calculation of SERS enhancement factors (EF)

- Estimation of the 4-MBA molecules within the bulk:

$$N_{bulk} = \frac{\rho V_{785} N_A}{M}$$

ρ : molecular density of 4-MBA

V_{785}: Laser-excited volume of the 4-MBA bulk material

N_A: Avogadro constant

M: Molar mass of 4-MBA

- Estimate of 4-MBA molecules adsorbed on the substrate (full coverage):

$$N_{SERS} = A_{785}\mu_s$$

A_{785}: Laser-irradiated surface

μ_s: Density of 4-MBA within a compact monolayer

$$\Rightarrow \frac{N_{bulk}}{N_{SERS}} = \frac{\rho V_{785} N_A}{M A_{785}\mu_s}$$

with $V_{785} = A_{785} z_{785}$

z_{785}: Depth of field

$$\Rightarrow \frac{N_{bulk}}{N_{SERS}} = \frac{\rho z_{785} N_A}{M\mu_s}$$

with ρ= 1.489 g/cm^3, M = 154 g/mol, μ_s= 5.263 nm^{-2} and z_{785} = 90µm.[3,4]

$$\Rightarrow \frac{N_{bulk}}{N_{SERS}} \approx 10^5$$

9. Polymer coating and characterization

The synthetic procedure followed to prepare the amphiphilic polymer, dodecylamine modified polyisobutylene-alt-maleic anhydride (PMA), was adapted from previous publications.[5–7] During preparation, 75% of the anhydride rings from the polyisobutylene-alt-maleic anhydride hydrophilic backbone were reacted with dodecylamine ligand, leaving 25% of them for further modification, such as incorporation of a dye. The polymer structure is shown in **Figure S14**:

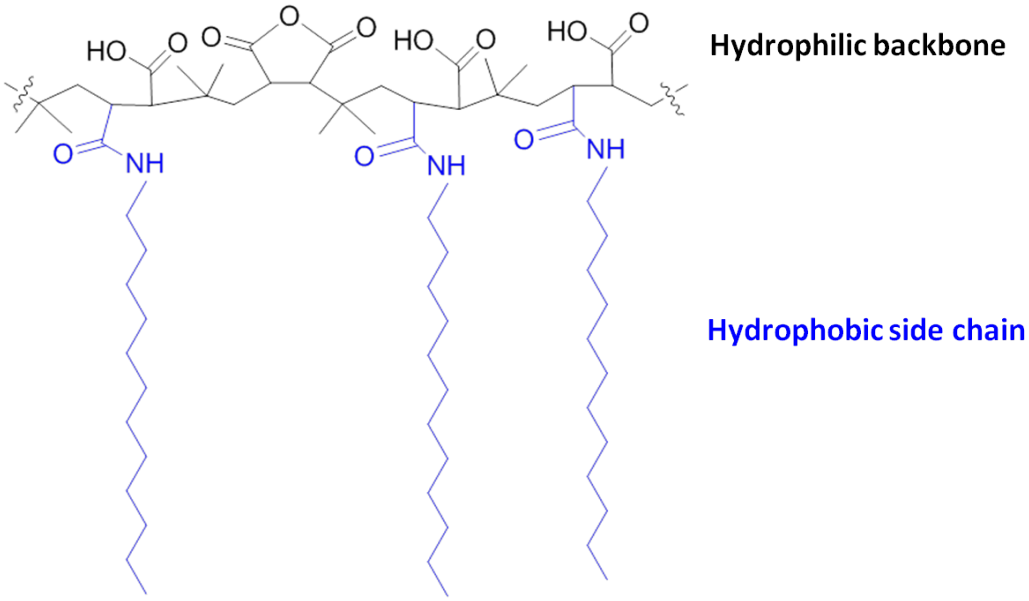

Figure S14. Structure of the amphiphilic polymer (PMA) comprising a hydrophilic backbone of polyisobutylene-alt-maleic anhydride (black) and a hydrophobic side chain of dodecylamine (blue).

After polymer coating, particles were washed several times by centrifugation (1730 g; 15 min; 20 ºC) and redispersed in Milli-Q water. Gel electrophoresis was used to ensure that all empty polymer micelles were removed. 1 wt% agarose gel was prepared by mixing agarose with tris-borate-EDTA buffer (TBE; 0.5x). Polymer coated AuNSs were mixed with glycerol to increase the sample density by placing the mixture in the cavity of the prepared gel. When an electric field of 18 $V \cdot cm^{-1}$ was applied to polymer coated NPs (negatively charged due to the carboxylic groups of the polymer), they migrated towards the "+" pole. After an hour a band of AuNSs was appreciated. Since empty polymer micelles move faster in the gel than NPs, they can be separated from each other (**Figure S15**).

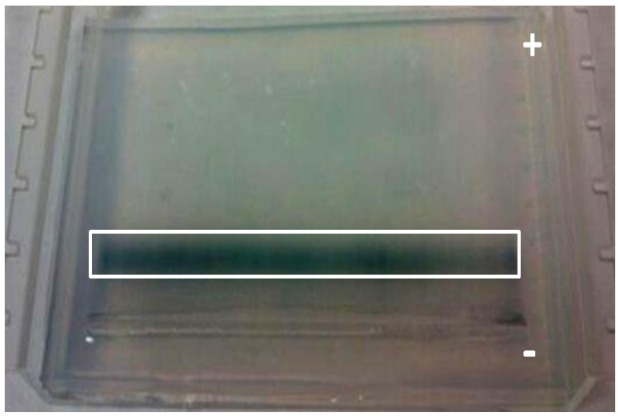

Figure S15. Image of an agarose gel in which polymer coated Au NSs had been run for 1 h under a potential of 18 $V \cdot cm^{-1}$. The signs "+" and "-" indicate the direction of the electric field. The marked section (white) indicates the area where the NPs accumulated.

TEM images show the preservation of the star-like shape after polymer coating. Negative staining of the sample was performed after a glow discharge treatment of the TEM grids for 2 min with air plasma. After placing the sample on the treated grid, 0.5 μL of a 0.5 wt% solution of uranyl acetate was added to the sample, providing contrast to differentiate the organic shell composed by DDT, PEG-SH and PMA. Confirmation that the white shell was not due to any artifact, serial focus imaging was performed, ranging from overfocused to underfocused images and confirming that the shell can in all cases be appreciated and Fresnel fringes appeared when the particle was under or over focus(**Figure S16**).

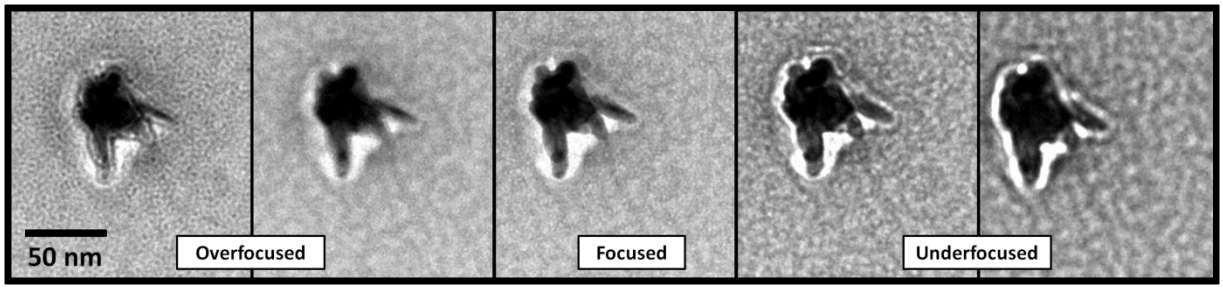

Figure S16. TEM focus series of negatively stained polymer coated Au NSs. The scale bar corresponds to 50nm.

10. References

(1) Templeton, A. C.; Hostetler, M. J.; Kraft, C. T.; Murray, R. W. Reactivity of Monolayer-Protected Gold Cluster Molecules: Steric Effects. *J. Am. Chem. Soc.***1998**, *120*, 1906–1911.

(2) Kelly, K. L.; Coronado, E.; Zhao, L. L.; Schatz, G. C. The Optical Properties of Metal Nanoparticles: The Influence of Size, Shape, and Dielectric Environment. *J. Phys. Chem. B***2003**, *107*, 668–677.

(3) Hrelescu, C.; Sau, T. K.; Rogach, A. L.; Jäckel, F.; Feldmann, J. Single Gold Nanostars Enhance Raman Scattering. *Appl. Phys. Lett.***2009**, *94*, 153113.

(4) Perassi, E. M.; Hrelescu, C.; Wisnet, A.; Döblinger, M.; Scheu, C.; Jäckel, F.; Coronado, E. A.; Feldmann, J. Quantitative Understanding of the Optical Properties of a Single, Complex-Shaped Gold Nanoparticle from Experiment and Theory. *ACS Nano***2014**, *8*, 4395–4402.

(5) Kaiser, U.; Aberasturi, D. J. de; Malinowski, R.; Amin, F.; Parak, W. J.; Heimbrodt, W. Multiplexed Measurements by Time Resolved Spectroscopy Using Colloidal CdSe/ZnS Quantum Dots. *Appl. Phys. Lett.***2014**, *104*, 041901.

(6) Lin, C.-A. J.; Sperling, R. A.; Li, J. K.; Yang, T.-Y.; Li, P.-Y.; Zanella, M.; Chang, W. H.; Parak, W. J. Design of an Amphiphilic Polymer for Nanoparticle Coating and Functionalization. *Small***2008**, *4*, 334–341.

(7) Pellegrino, T.; Manna, L.; Kudera, S.; Liedl, T.; Koktysh, D.; Rogach, A. L.; Keller, S.; Rädler, J.; Natile, G.; Parak, W. J. Hydrophobic Nanocrystals Coated with an Amphiphilic Polymer Shell: A General Route to Water Soluble Nanocrystals. *Nano Lett.***2004**, *4*, 703–707.